Model-Based Control Can Improve the Performance of Artificial Cilia

Edoardo Milana[1,2], Francesco Stella[3], Benjamin Gorissen[2,4], Dominiek Reynaerts[2], Cosimo Della Santina[3,5]

***Abstract*— Artificial cilia are a prominent example of physical intelligence. Their mechanical properties are often designed so to achieve desired motions in response to very simple actuation patterns. Yet, variability in the mechanical properties are inherent in these systems. This may critically disrupt the input-output relation, resulting in a final behavior completely different from the desired one. In this Communication we investigate the possibility of designing a *robotic brain* that helps the cilium to maintain its physical intelligence. We achieve that by closing a model-based control loop which tracks the position of the end effector while compensating for drag forces. We propose experiments to characterize our model, and extensive simulations validating the results in different conditions. This work is intended as a proof of concept, which will be further expanded in future work.**

I. Introduction

Biological cilia are slender hair-like organelles protruding from eukaryotic cells, and their motion is responsible for fluid transport at such micro-scales [1]. Given the size, the hydrodynamic conditions are described by Reynolds numbers much smaller than one. In these conditions, a body must cyclically deform with a nonreciprocal pattern in order to generate a net fluid flow, as consequence of the Scallop theorem [2]. Biological cilia are an excellent source of inspiration for small-scale soft robots [3] immersed in fluids. Given their typical bent deformation, soft bending microactuators are widely used to build artificial cilia [4]–[6]. Sareh et al. [7] showed that a multi-segment configuration of bending actuators can accurately mimic the asymmetric motion of the cilium. The spatial asymmetry of the single cilium beat is caused by the different kinematics of the recovery stroke compared to the effective stroke. It follows that the tip trajectory of the cilium draws a closed area, named "swept area", that quantifies the degree of asymmetry. Khaderi et al. [8] revealed that there is a linear relationship between the amount of swept area and the net flow induced by the cilium. In previous works [9], we reported on the low Reynolds fluid propulsion generated by the biomimetic asymmetric motions of bi-segment soft pneumatic artificial cilia. In the latter case, the soft cilia were actuated with very simple pressure patterns. The resulting desired oscillatory behavior is therefore an emergent characteristics of the soft body [10].

Yet, solving the problem by completely relying on phyisical intelligence has two limitations. First, it does not allow for any change in the cilia trajectory or frequency of oscillation. Secondly, the unavoidable differences that exist between the ideal design and the actual physical robot may change drastically the resulting open loop response. In turn, these two factors may result in sub-optimal behaviors of the cilia. Both these limitations can be addressed by augmenting the intelligent body with a suitable soft robotic brain. This can be done by means of model-based feedback control. The application of this class of techniques to soft robotics flourished in the last few years [11]–[16], thanks to the development of compact but effective dynamic models for soft robots [17]–[19]. A model-free control loop achieving synchronizations across multiple cilia has been proposed in [20], [21]. There, the focus is not on the performance of a single cilium. In this work, we implement a controller based on the dynamic Piecewise Constant Curvature (PCC) model introduced in [22]. The controller is designed so to enable trajectory tracking of the tip of the cilia. We show that in this way the swept area of the cilia can be strongly enlarged, and kept constant across oscillation frequencies.

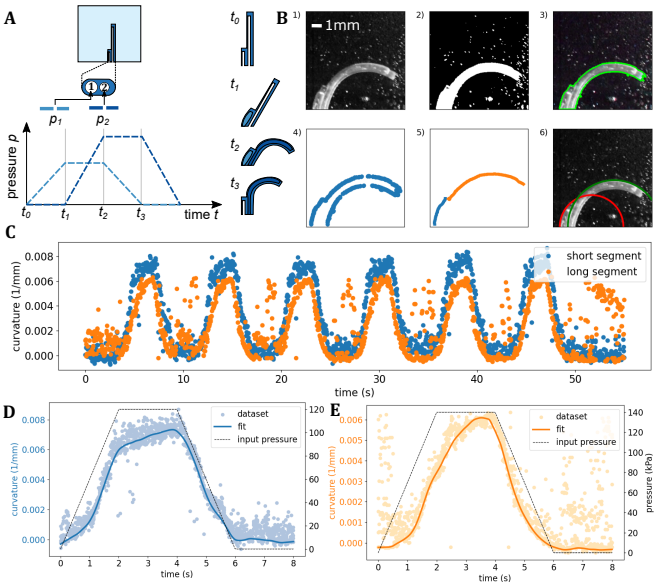

Fig. 1. A. Artificial cilium actuation scheme. B. Image analysis steps to measure the segments curvature. C. Segments curvature measurements over six cycles. D. Dataset combined in one cycle and fit for the short segment. E. Dataset combined in one cycle and fit for the long segment.

II. Experiments

The artificial cilium considered in this work is composed of two soft inflatable bending segments merged in a monolithic structure (see Figs. 1 A and B). The bending segment is a PDMS pillar with an inner eccentric inflatable cavity. The eccentricity determines a stiffness asymmetry of the cross-section which cause the pillar to bend when inflated. More details on the operation and manufacturing of those artificial

[1] Institute for the Protection of Terrestrial Infrastructures, German Aerospace Center (DLR), Sankt Augustin, Germany. [2] Department of Mechanical Engineering, KU Leuven and Flanders Make, Leuven, Belgium [3] Cognitive Robotics Department, 3ME, TU Delft, Delft, Netherlands. [4] J.A. Paulson School of Engineering and Applied Sciences, Harvard University, Cambridge, MA 02138, USA [5] Institute of Robotics and Mechatronics, German Aerospace Center (DLR), Oberpfaffenhofen, Germany.

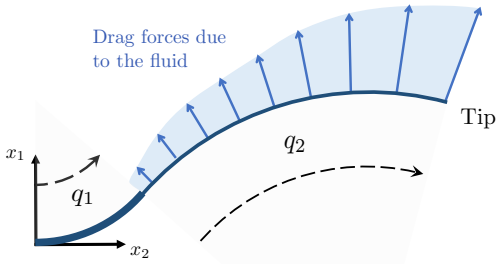

Fig. 2. Schematic representation of the proposed model. The shape of the cilia is described with two segments with constant curvature (q_1 and q_2 respectively). The aim of our controller is to impose a desired evolution to the tip by controlling the input pressure, despite the drag forces generated by the fluid.

cilia can be found in [23]. The two degrees of freedom of the bi-segment configuration are necessary to create the cilia asymmetric motion. By actuating the two segments following the pattern in Fig. 1A, the tip of the cilium follows an asymmetric trajectory. To mimic the fluid dynamic conditions of biological cilia ($Re < 1$), the artificial cilia are submerged in glycerol (viscosity $\mu = 1.412$ Pa s).

A. Dynamic Model

The use of PCC kinematic models to describe the shape of a cilia has been already validated in [24]. We consider here a complete dynamic model augmented with a simple model of robot-fluid interaction. Fig. 2 shows a schematic representation of the model of the cilia, where the main quantities are highlighted. Each bending segment is described with a segment having curvature q and length constant in space. The shape is therefore a semi-circle. The curvature q may vary in time, while the length is constant. Therefore, the state of the cilia is $(q_1, q_2, \dot{q}_1, \dot{q}_2)$. We propose to model the dynamics of the cilia in the following form

$$M(q_1,q_2)\begin{bmatrix}\ddot{q}_1\\ \ddot{q}_2\end{bmatrix} + C(q_1,q_2,\dot{q}_1,\dot{q}_2)\begin{bmatrix}\dot{q}_1\\ \dot{q}_2\end{bmatrix} + \begin{bmatrix}k_1 q_1\\ k_2 q_2\end{bmatrix} + \begin{bmatrix}d_1(q_1)\dot{q}_1\\ d_2(q_2)\dot{q}_2\end{bmatrix} = \begin{bmatrix}a_1 P_1\\ a_2 P_2\end{bmatrix}. \tag{1}$$

$M(q_1, q_2) \in \mathbb{R}^{2\times 2}$ is the inertia matrix, and $C(q_1, q_2, \dot{q}_1, \dot{q}_2) \in \mathbb{R}^{2\times 2}$ collects Coriolis and centrifugal terms. These are evaluated by connecting an equivalent mass in the geometrical center of mass of the segment, as discussed in [25]. We add here also a rotational inertia. The two constants $k_1, k_2 > 0$ are the flexural stiffness of the segments. The area factors $a_1, a_2 > 0$ map input pressures P_1, P_2 into generalized forces at the curvature level. The equivalent damping of each segment is configuration dependent: $d_1(q_1), d_2(q_2)$. Consider the infinitesimal elements at distance s from the base of a constant curvature segment. Its Cartesian velocity is $v_s \in \mathbb{R}^2$. The element experiences a drag force $-dv_s$ due to the fluid, with $d \in \mathbb{R}$ being a constant connected to the fluid viscosity [26]. This generates a distribution of infinitesimal forces, as shown in Fig. 2. The total force experienced by the segment is $d\left(\int_0^L J_s^{\mathrm{T}} J_s \mathrm{d}s\right)\dot{q}$, where J_s is the Jacobian mapping the variation of curvature into Cartesian velocity, and $\dot{q} = (\dot{q}_1, \dot{q}_2)$. As a trade off between accuracy and precision, we consider the 5^{th} order approximation of the drag forces.

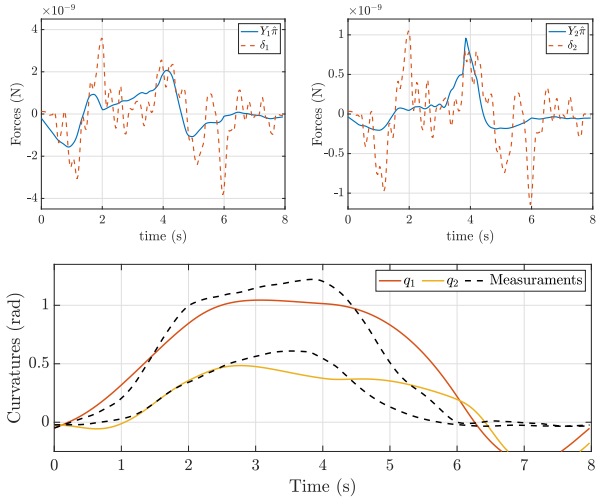

Fig. 3. The proposed model well explains the experimental data. Top panels show the difference between the rows of δ and $Y\pi$ (i.e. what we are actively optimizing for). Note that the variability of δ may be an artifact of the noise in the measurements amplified by numerical differentiation. The bottom panel shows the simulated evolution compared to the real data.

This yields the following

$$d_i(q_i) \simeq d_{0,i} + d_{2,i} q_i^2 + d_{4,i} q_i^4 > 0, \tag{2}$$

where $d_{0,i}, d_{2,i}, d_{4,i} \in \mathbb{R}$ are constants. In this way $d_{0,i}$ can also include the usual linear damping generated by the robot's body itslef. Note that odd terms are not appearing since the $J_s^{\mathrm{T}} J_s$ is even.

B. Data Acquisition

The segments are synchronously driven with a trapezoidal pressure wave (maximum pressure of 140 kPa for the long segment and 120 kPa for the short) for six cycles with a period of 8 s. A camera is placed in front of the cilium, capturing the motion at 25 frames/s. The video is analysed through a computer vision algorithm written in python using the OpenCV library to extract the two curvature segments. The image analysis steps are depicted in 1B. For each frame (subfigure 1), the image is binarized (subfigure 2) and the larger contour is detected (subfigure 3) and extracted (subfigure 4). Only the upper profile is selected and segmented to obtain the two actuators profiles (subfigure 5). Note that the resulting shapes are remarkably close to the arcs of a circle. This is the instant of maximum velocity, and therefore the point in which the PCC hypothesis should be less accurate. Finally, the segmented profiles are fitted through a circle using a least-square fitting (subfigure 6). Figure 1C depicts curvature measurements for each frame. The overall curvature trends are consistent and coherent. The reconstruction of the long segment straight configuration is not precise due to the well known numerical instability of the PCC model. The collected dataset of the six cycles is grouped in a single cycle and fit to a curve. In Figs. 1 D and E, the pressure profile is superimposed to the curvature measurements using the acoustic signal generated by the pressure valves.

C. Identification

The elements of the dynamic model (1) depend on several physical quantities. Some of them can be di-

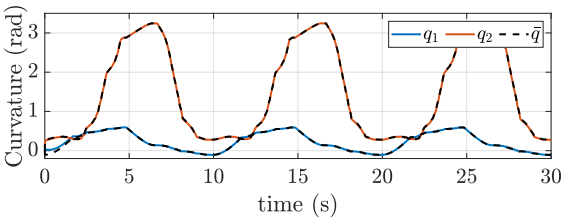

Fig. 4. An example of evolution of the curvature in time. The low level generates the pressures necessary to make the actual curvature q follow the desired curvature $\bar{q}$. Convergence happens in less than one second.

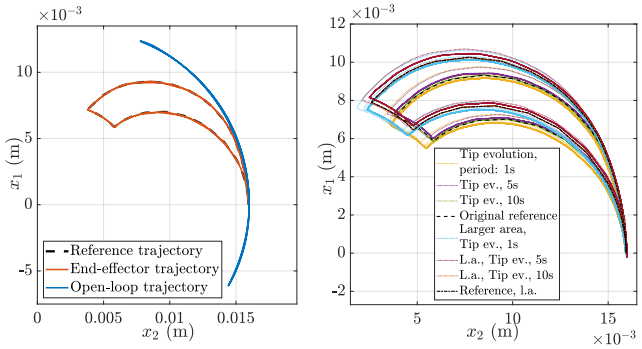

Fig. 5. End effector swept area evolution in Cartesian coordinates. The left panel shows that the proposed feedback strongly improves the ability of the cilia to follow the desired trajectory. The right panel reports the performance of the controller for various frequencies and a larger path.

rectly measured. Others are obtained through an experimental characterization of the two segments. In this work we consider the following parameters as unknowns: k_1, k_2,$d_{0,1}, d_{0,2}, d_{2,1}$,$d_{2,2}, d_{4,1}, d_{4,2}$, a_1, a_2. We call π the vector collecting these parameters. We instead measure lengths, masses, inertias. Thus we can re-write the dynamics as $\delta(q_1, q_1, \dot{q}_1, \dot{q}_2, \ddot{q}_1, \ddot{q}_2) = Y(q_1, q_2, \dot{q}_1, \dot{q}_2, P_1, P_2)\pi$, where δ collects the first two terms in (1) - the dynamic forces - and Y is such that $Y\pi$ collects all the remaining terms. We call $\tilde{q}_1, \tilde{q}_2$ $\tilde{P}_1, \tilde{P}_2$ the measurements of curvature and pressure gathered in the above discussed experiments. We call $t_1, \ldots, t_m$ the instances during which the measurements are done. We evaluate the set of parameters that better explain the real data by minimizing the least mean square error of $||\delta - Y\pi||_2^2$ across all data. This is achieved by

$$\hat{\pi} = \begin{bmatrix} Y(\tilde{q}_1(t_1), \ldots, \tilde{P}_2(t_1)) \\ \vdots \\ Y(\tilde{q}_1(t_m), \ldots, \tilde{P}_2(t_m)) \end{bmatrix}^+ \begin{bmatrix} \delta(\tilde{q}_1(t_1), \ldots, \ddot{\tilde{q}}_2(t_1)) \\ \vdots \\ \delta(\tilde{q}_1(t_m), \ldots, \ddot{\tilde{q}}_2(t_m)) \end{bmatrix}, \quad (3)$$

where $\cdot^+$ is the Moore-Penrose pseudo-inverse. Time derivatives are calculated through numerical differentiation. Fig. 3 shows the result of this identification procedure.

III. Model Based Controller

The controller that we propose here is an extension of the one proposed in [27], [28], which we adapt here to act on (1). This required some modifications, like the introduction of a compensation for fluid-induced dissipation. The controller is organized in two stages. First, the reference trajectory in curvature space $\bar{q} = (\bar{q}_1, \bar{q}_2)$ required to generate the desired tip evolution $\bar{x} \in \mathbb{R}^2$ is calculated as solution of the following dynamical system

$$\dot{\bar{q}} = J_{\text{tip}}^{-1}(\bar{q})[\dot{\bar{x}} - \kappa(\bar{x} - h(\bar{q}))] \quad (4)$$

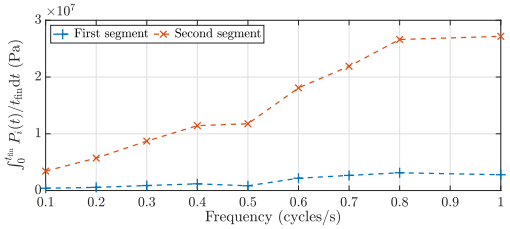

Fig. 6. Average control pressure (equation) for performing the task with different cycles per second. Increasing the number of cycles generates higher velocities and accelerations, which leads to higher torques.

where h is the forward kinematics of the cilia's tip, and $J_{\text{tip}} = \partial h / \partial \bar{q}$. In this work we take $\kappa = 10$. The acceleration can be evaluated by direct differentiation of (4), which yields $\ddot{\bar{q}} = J_{\text{tip}}^{-1}[\ddot{\bar{x}} - \kappa^2(\bar{x} - h(\bar{q}))] - J_{\text{tip}}^{-1}\dot{J}J_{\text{tip}}^{-1}[\dot{\bar{x}} - \kappa(\bar{x} - h(\bar{q}))]$, where we omitted explicit dependencies on $\bar{q}$ and $\dot{\bar{q}}$. We also expressed the time derivative of J_{tip}^{-1} as $J_{\text{tip}}^{-1}\dot{J}J_{\text{tip}}^{-1}$, see for example [29]. The second part of the controller generates the pressures $P = (P_1, P_2)$ from the knowledge of $q, \dot{q}, \bar{q}, \dot{\bar{q}}, \ddot{\bar{q}}$. The goal is to make q converge to $\bar{q}$. The controller is

$$P = \begin{bmatrix} 1/a_1 & 0 \\ 0 & 1/a_2 \end{bmatrix} \Bigg(C(q, \dot{q}) \begin{bmatrix} \dot{q}_1 \\ \dot{q}_2 \end{bmatrix} + \begin{bmatrix} k_1 q_1 \\ k_2 q_2 \end{bmatrix} + \begin{bmatrix} d_1(q_1)\dot{q}_1 \\ d_2(q_2)\dot{q}_2 \end{bmatrix} + M(q, \dot{q})(\ddot{\bar{q}} + \kappa_{\text{D}}(\dot{\bar{q}} - \dot{q}) + \kappa_{\text{P}}(\bar{q} - q)) \Bigg), \quad (5)$$

where all elements are as in (1) and $\kappa_{\text{P}}, \kappa_{\text{D}}$ are two positive control gains. In the following we take both equal to 100.

With the proposed controller, we aim at following a trajectory with the end effector which covers a region with a large swept area (see Sec. I). More specifically, we select the area that was originally considered in the design of the cilia [23]. This still leaves free the frequency of oscillation. We start by considering a frequency of one cycle every 10 seconds (as in Sec. II). Fig. 4 reports the desired curvature evolution $\bar{q}$ generated by (4), and the evolution of the actual curvature q produced by (5). Fig. 5a shows the trajectory generated at the end effector by the proposed controller, compared with the open loop excitation in Sec. II. The controller generates a dramatic improvement of performance. This is consistent across frequencies, up to 1 cycle per second, as shown in Fig. 5b. The same panel shows what happens when we test the effectiveness of the algorithm with a larger area (approximately 10% larger). In all conditions the trajectory is closely tracked at steady state. This proves that the proposed control algorithm can be used not only to recover ideal performance, but also to improve upon the original design idea. Finally, Fig. 6 shows the average pressure that is exerted by the controller during the task.

IV. Conclusions and Future Work

This Communication showed through a *proof of concept* application, that model based closed loop control can be used to augment the performance of physically intelligent artificial cilia. Future work will be devoted to validating the method in full-fledged swimming tasks, as for example in [30]. Extension of the controller will be considered to models with affine curvature [31], to online adaption to different fluid conditions [32].

REFERENCES

[1] C. Brennen and H. Winet, "Fluid mechanics of propulsion by cilia and flagella," *Annual Review of Fluid Mechanics*, vol. 9, no. 1, pp. 339–398, 1977.

[2] E. M. Purcell, "Life at low Reynolds number," *Am. J. Phys.*, vol. 45, pp. 3–11, 1977. [Online]. Available: http://www.damtp.cam.ac.uk/user/gold/pdfs/purcell.pdf

[3] C. Della Santina, M. G. Catalano, and A. Bicchi, *Soft Robots*. Berlin, Heidelberg: Springer Berlin Heidelberg, 2020, pp. 1–14.

[4] B. Gorissen, M. De Volder, and D. Reynaerts, "Pneumatically-actuated artificial cilia array for biomimetic fluid propulsion," *Lab on a Chip*, vol. 15, no. 22, pp. 4348–4355, 2015.

[5] H. Gu, Q. Boehler, H. Cui, E. Secchi, G. Savorana, C. De Marco, S. Gervasoni, Q. Peyron, T.-Y. Huang, S. Pane *et al.*, "Magnetic cilia carpets with programmable metachronal waves," *Nature communications*, vol. 11, no. 1, pp. 1–10, 2020.

[6] X. Dong, G. Z. Lum, W. Hu, R. Zhang, Z. Ren, P. R. Onck, and M. Sitti, "Bioinspired cilia arrays with programmable nonreciprocal motion and metachronal coordination," *Science advances*, vol. 6, no. 45, p. eabc9323, 2020.

[7] S. Sareh, J. Rossiter, A. Conn, K. Drescher, and R. E. Goldstein, "Swimming like algae: biomimetic soft artificial cilia." *J. R. Soc. Interface*, vol. 10, no. 78, pp. 20 120 666–, 2012. [Online]. Available: http://rsif.royalsocietypublishing.org/content/10/78/20120666

[8] S. N. Khaderi, M. G. H. M. Baltussen, P. D. Anderson, J. M. J. Den Toonder, and P. R. Onck, "Breaking of symmetry in microfluidic propulsion driven by artificial cilia," *Phys. Rev. E - Stat. Nonlinear, Soft Matter Phys.*, vol. 82, no. 2, 2010.

[9] E. Milana, B. Gorissen, S. Peerlinck, M. De Volder, and D. Reynaerts, "Artificial Soft Cilia with Asymmetric Beating Patterns for Biomimetic Low-Reynolds-Number Fluid Propulsion," *Adv. Funct. Mater.*, vol. 1900462, pp. 1–8, 2019.

[10] H. Hauser, A. J. Ijspeert, R. M. Füchslin, R. Pfeifer, and W. Maass, "Towards a theoretical foundation for morphological computation with compliant bodies," *Biological cybernetics*, vol. 105, no. 5, pp. 355–370, 2011.

[11] C. Duriez, "Control of elastic soft robots based on real-time finite element method," in *2013 IEEE international conference on robotics and automation*. IEEE, 2013, pp. 3982–3987.

[12] B. Deutschmann, A. Dietrich, and C. Ott, "Position control of an underactuated continuum mechanism using a reduced nonlinear model," in *2017 IEEE 56th Annual Conference on Decision and Control (CDC)*. IEEE, 2017, pp. 5223–5230.

[13] C. M. Best, L. Rupert, and M. D. Killpack, "Comparing model-based control methods for simultaneous stiffness and position control of inflatable soft robots," *The International Journal of Robotics Research*, p. 0278364920911960, 2020.

[14] H.-S. Chang, U. Halder, C.-H. Shih, A. Tekinalp, T. Parthasarathy, E. Gribkova, G. Chowdhary, R. Gillette, M. Gazzola, and P. G. Mehta, "Energy shaping control of a cyberoctopus soft arm," in *2020 59th IEEE Conference on Decision and Control (CDC)*. IEEE, 2020, pp. 3913–3920.

[15] M. Thieffry, A. Kruszewski, T.-M. Guerra, and C. Duriez, "Lpv framework for non-linear dynamic control of soft robots using finite element model," in *IFAC 2020 - 21rst IFAC World Congress, Jul 2020, Berlin, Germany*, 2020.

[16] E. Franco, A. G. Casanovas, and A. Donaire, "Energy shaping control with integral action for soft continuum manipulators," *Mechanism and Machine Theory*, vol. 158, p. 104250, 2021.

[17] S. Grazioso, G. Di Gironimo, and B. Siciliano, "A geometrically exact model for soft continuum robots: The finite element deformation space formulation," *Soft robotics*, vol. 6, no. 6, pp. 790–811, 2019.

[18] F. Renda, C. Armanini, V. Lebastard, F. Candelier, and F. Boyer, "A geometric variable-strain approach for static modeling of soft manipulators with tendon and fluidic actuation," *IEEE Robotics and Automation Letters*, vol. 5, no. 3, pp. 4006–4013, 2020.

[19] S. Sadati, S. E. Naghibi, L. Da Cruz, and C. Bergeles, "Reduced-order modeling and model order reduction for soft robots," *ArXiv*, 2021.

[20] M. Elshalakani and C. H. Brücker, "Spontaneous synchronization of beating cilia: An experimental proof using vision-based control," *Fluids*, vol. 3, no. 2, p. 30, 2018.

[21] M. Elshalakani and C. Brücker, "Simulation of self-coordination in a row of beating flexible flaplets for micro-swimmer applications: Model and experiment study," *Journal of Fluids and Structures*, vol. 94, p. 102923, 2020.

[22] C. Della Santina, R. K. Katzschmann, A. Biechi, and D. Rus, "Dynamic control of soft robots interacting with the environment," in *2018 IEEE International Conference on Soft Robotics (RoboSoft)*. IEEE, 2018, pp. 46–53.

[23] E. Milana, R. Zhang, M. R. Vetrano, S. Peerlinck, M. De Volder, P. R. Onck, D. Reynaerts, and B. Gorissen, "Metachronal patterns in artificial cilia for low reynolds number fluid propulsion," *Science Advances*, vol. 6, no. 49, p. eabd2508, 2020.

[24] S. Sareh, J. Rossiter, A. Conn, K. Drescher, and R. E. Goldstein, "Swimming like algae: biomimetic soft artificial cilia," *Journal of the Royal Society Interface*, vol. 10, no. 78, p. 20120666, 2013.

[25] C. Della Santina, R. K. Katzschmann, A. Bicchi, and D. Rus, "Model-based dynamic feedback control of a planar soft robot: trajectory tracking and interaction with the environment," *The International Journal of Robotics Research*, vol. 39, no. 4, pp. 490–513, 2020.

[26] F. Renda, M. Giorelli, M. Calisti, M. Cianchetti, and C. Laschi, "Dynamic model of a multibending soft robot arm driven by cables," *IEEE Trans. Robot.*, vol. 30, no. 5, pp. 1109–1122, 2014.

[27] C. Della Santina, A. Bicchi, and D. Rus, "Dynamic control of soft robots with internal constraints in the presence of obstacles," in *2019 IEEE/RSJ International Conference on Intelligent Robots and Systems (IROS)*. IEEE, 2019, pp. 6622–6629.

[28] J. Hughes, C. Della Santina, and D. Rus, "Extensible high force manipulator for complex exploration," in *2020 3rd IEEE International Conference on Soft Robotics (RoboSoft)*. IEEE, 2020, pp. 733–739.

[29] K. B. Petersen and M. S. Pedersen, "The matrix cookbook," Oct. 2008, version 20081110.

[30] C. Huang, J.-a. Lv, X. Tian, Y. Wang, Y. Yu, and J. Liu, "Miniaturized swimming soft robot with complex movement actuated and controlled by remote light signals," *Scientific reports*, vol. 5, no. 1, pp. 1–8, 2015.

[31] C. Della Santina, "The soft inverted pendulum with affine curvature," in *2020 59th IEEE Conference on Decision and Control (CDC)*. IEEE, 2020, pp. 4135–4142.

[32] M. Trumić, C. Della Santina, K. Jovanović, and A. Fagiolini, "Adaptive control of soft robots based on an enhanced 3d augmented rigid robot matching," *IEEE Control Systems Letters*, 2020.